

ARTICLE



Celsr2 regulates NMDA receptors and dendritic homeostasis in dorsal CA1 to enable social memory

Bailing Chen^{1,2,8}, Laijian Wang^{3,8}, Xuejun Li^{1,8}, Zhe Shi^{4,8}, Juan Duan¹, Ji-an Wei¹, Cunzheng Li¹, Chaoqin Pang¹, Diyang Wang¹, Kejiao Zhang¹, Hao Chen¹, Wanying Na¹, Li Zhang¹, Kwok-Fai So^{1,2,5}, Libing Zhou¹, Bin Jiang¹, Ti-Fei Yuan^{1,6,7} and Yibo Qu^{1,2,5}

© The Author(s), under exclusive licence to Springer Nature Limited 2022

Social recognition and memory are critical for survival. The hippocampus serves as a central neural substrate underlying the dynamic coding and transmission of social information. Yet the molecular mechanisms regulating social memory integrity in hippocampus remain unelucidated. Here we report unexpected roles of Celsr2, an atypical cadherin, in regulating hippocampal synaptic plasticity and social memory in mice. *Celsr2*-deficient mice exhibited defective social memory, with rather intact levels of sociability. In vivo fiber photometry recordings disclosed decreased neural activity of dorsal CA1 pyramidal neuron in *Celsr2* mutants performing social memory task. *Celsr2* deficiency led to selective impairment in NMDAR but not AMPAR-mediated synaptic transmission, and to neuronal hypoactivity in dorsal CA1. Those activity changes were accompanied with exuberant apical dendrites and immaturity of spines of CA1 pyramidal neurons. Strikingly, knockdown of *Celsr2* in adult hippocampus recapitulated the behavioral and cellular changes observed in knockout mice. Restoring NMDAR transmission or CA1 neuronal activities rescued social memory deficits. Collectively, these results show a critical role of *Celsr2* in orchestrating dorsal hippocampal NMDAR function, dendritic and spine homeostasis, and social memory in adulthood.

Molecular Psychiatry; <https://doi.org/10.1038/s41380-022-01664-x>

INTRODUCTION

The accurate discrimination of familiar and novel conspecifics is required for appropriate social behavior, which is crucial for group cohesion, reproduction and survival. Social memory, the ability to recognize and memorize a social partner, depends on the appropriate function of several brain regions such as the hippocampus, medial prefrontal cortex (mPFC), anterior cingulate cortex (ACC) and amygdala [1, 2]. The hippocampus, especially, regulates different and complementary aspects of social memory. Ventral CA1 is important for social memory storage [3], whereas dorsal CA1 is crucial for formation of short-term social memory [4, 5], and CA2 is involved in social information processing [6, 7]. However, thus far, the molecular mechanisms by which the hippocampus regulates the formation and function of social memory remain elusive. Of note, N-methyl-D-aspartate receptor (NMDAR) function and associated changes in synaptic plasticity are recognized as important cellular mechanisms supporting social memory [8].

Atypical cadherins Celsr1-3 play important roles in neural development [9]. Among them, Celsr2 regulates ciliogenesis, neuronal migration, axon outgrowth and regeneration, and dendrite deployment [10–15]. Contrary to its paralogs Celsr1 and Celsr3,

Celsr2 remains strongly expressed in the adult brain [16], indicating potential roles in regulating neural homeostasis in the adult [17]. Human genetic studies reported the association of *Celsr2* polymorphism with schizophrenia, autism and Joubert Syndrome, all of which exhibit deficits in social memory [18–22]. It is unclear whether *Celsr2* regulates social memory through its developmental effects or during adulthood. In addition, the molecular and cellular substrates underlying such behavioral alterations have not been elucidated.

As *Celsr2* mutant mice develop and survive as adults, we investigated their behavioral performances in standard tests, and found clear evidence of a deficit in social recognition memory that we investigated further. We first confirmed the persistent expression of *Celsr2* in the adult mouse hippocampus. Absence of *Celsr2* resulted in reduced NMDAR mediated synaptic transmission and hypoactivity of CA1 pyramidal neurons in response to novel conspecifics, a hallmark of social memory deficits. *Celsr2* deficiency also led to dendrite overgrowth and impaired spine maturation in hippocampal CA1 pyramidal neurons. Selective deletion of *Celsr2* in adult dorsal CA1 recapitulated both synaptic dysfunction and social memory deficits observed in knockout (KO) mice, suggesting that

¹Key Laboratory of CNS Regeneration (Ministry of Education), Guangdong-Hong Kong-Macao Institute of CNS Regeneration, Jinan University, Guangzhou 510632, China. ²Co-innovation Center of Neuroregeneration, Nantong University, Nantong, Jiangsu, China. ³Guangdong Province Key Laboratory of Brain Function and Disease, Zhongshan School of Medicine, Sun Yat-sen University, Guangzhou, China. ⁴Key Laboratory for Quality Evaluation of Bulk Herbs of Hunan Province, Hunan University of Chinese Medicine, Changsha, Hunan 410208, China. ⁵Guangdong-Hong Kong-Macao Greater Bay Area Center for Brain Science and Brain-Inspired Intelligence, Guangzhou 510515, China. ⁶Shanghai Key Laboratory of Psychotic Disorders, Shanghai Mental Health Center, Shanghai Jiao Tong University School of Medicine, Shanghai, China. ⁷Shanghai Key Laboratory of Anesthesiology and Brain Functional Modulation, Translational Research Institute of Brain and Brain-Like Intelligence, Shanghai Fourth People's Hospital Affiliated to Tongji University School of Medicine, Shanghai, China. ⁸These authors contributed equally: Bailing Chen, Laijian Wang, Xuejun Li, Zhe Shi. [✉]email: jiangb3@mail.sysu.edu.cn; ytf0707@126.com; tqyibo@jnu.edu.cn

Received: 21 March 2022 Revised: 31 May 2022 Accepted: 7 June 2022

Published online: 04 July 2022

Celsr2 maintains adult hippocampal circuit integrity. Our results reveal previously unknown roles of Celsr2 in social memory, through regulation of NMDA receptor function and synaptic plasticity.

MATERIALS AND METHODS

Animals

All animal experimental protocols were approved by the Ethics Committee of Experimental Animals of Jinan University in accordance with Institutional Animal Care and Use Committee guidelines for animal research. The *Celsr2*^{LacZ/+} mice [10], *Celsr2*^{-/-} mice [12], *Celsr2*^{ff} mice [12], *Thy1-YFP* mice [23], *Rosa26*^{Tom} mice [24] and *Nestin-CreER*^{T2} mice [25] were described and validated previously. *Celsr2*^{-/-}; *Thy1-YFP*, *Celsr2*^{ff}; *Thy1-YFP*, *Celsr2*^{ff/+}; *Rosa26*^{Tom}; *Nestin-CreER*^{T2}, *Celsr2*^{-/-}; *Rosa26*^{Tom}; *Nestin-CreER*^{T2}, and *Celsr2*^{ff/+}; *Rosa26*^{Tom}; *Nestin-CreER*^{T2} mice were bred from parental lines. All mice were maintained under a 12 h light/dark cycle (lights on at 08:00, off at 20:00) with food and water *ad libitum*. The sample size was determined based on literatures from the same field, and in consideration of animal size limit due to animal welfare requirements and animal experimental ethical code. Although no systemic randomization method was used, animals were assigned randomly into each group.

Immunofluorescence staining

Mice were anesthetized using 1.25% Avertin and were perfused with 4% paraformaldehyde. 16 μ m cryostat sections for β -gal staining and 40 μ m vibratome sections for c-Fos staining were used. After PBS washing and BSA blocking, the brain sections were incubated with primary antibody at 4 °C overnight, followed by secondary antibody. Primary antibodies used: chicken anti- β -gal (1: 250; Abcam, ab9361), rabbit anti-NeuN (1: 1000; Abcam, ab177487), rabbit anti-c-Fos (1: 1000; Cell Signaling Technology, 2250), rabbit anti-NG (1: 500; Millipore, AB5620), rabbit anti-GABA (1: 500; Sigma, A2052), mouse anti-PV (1: 1000; Swant, 235), mouse anti-CR (1: 500; Swant, 6B3), mouse anti-CB (1: 500; Sigma, C9848). Fluorescent secondary antibodies used: goat anti-chicken IgY with Alexa Fluor 594 (1: 1000; Invitrogen, A11042), donkey anti-rabbit IgG with Alexa Flour 488 (1: 1000; Invitrogen, A21206), donkey anti-rabbit IgG with Alexa Flour 594 (1: 1000; Invitrogen, A21207), donkey anti-mouse IgG with Alexa Flour 488 (1: 1000; Invitrogen, A21202). The fluorescent images were captured with a fluorescence microscope (ZEISS, Germany).

Behavioral tests

All the mice for behavioral tests were housed in groups, 4–6 mice per cage. All behavioral tests were performed during the light phase of the cycle between 09:00 and 17:00. Mice were allowed 1 h to habituate to the testing rooms before behavioral tests. Experimenters were blind to the genotype when behavioral tests were carried out. Male mice at 8–10 weeks of age were used for all the behavior tests. The number of mice per group is indicated in the figures.

Test for social interaction and social novelty: The social test for sociability and social novelty was performed as described previously [3]. Briefly, 8–10-week-old male *Celsr2* KO or cKO mice and wild-type (WT) littermate controls were used. 4–5-week-old WT male mice were used as strangers 1 and 2. In the beginning, the test mouse was put in the center of the arena and left to habituate for 5 min. For the sociability test, stranger 1 was introduced into a wire cage (the diameter = 10 cm) on the left side and the other same wire cage on the right side was empty. The test mouse was allowed to explore freely for 5 min to become familiar with the stranger 1 mouse. Following this, stranger 2 was introduced into the previously empty wire cage and again the test mouse was allowed to freely explore the chamber for 5 min. Time spent on each cage and the test mouse's trajectory were recorded using SocialScan software (Clever System Inc.).

Stereotaxic surgery

Mice were anesthetized using 1.25% Avertin. After local sterilization and incision of head skins, the dorsal hippocampal CA1 was localized under a stereotaxic instrument (RWD Life Science Inc., China). The stereotaxic coordinates for dorsal CA1 injection were anterior posterior (AP) 2.00, medial lateral (ML) 1.80 and dorsal ventral (DV) 1.50 mm. After drilling a hole by the high-speed microdrill, viral injection into CA1 was performed at a rate of 50 nl min⁻¹ using a glass micropipette connected to an ultramicro injection pump (Nanoliter 2010, World Precision Instruments, Sarasota, USA). The micropipette was retained for 10 min before retraction. The head skin was closed for post-surgery monitor. 150 nl of AAV2/9-CaMKIIα-GCaMP6s-

WPRE-hGH pA (viral titer, 5.24 × 10¹² genome copies/ml; Taitool Bioscience, China) for *in vivo* two-photon calcium imaging or AAV2/9-CaMKIIα-GCaMP6m-WPRE-hGH pA (viral titer, 2.81 × 10¹² genome copies/ml; Taitool Bioscience, China) for *in vivo* Ca²⁺ fiber photometry was unilaterally injected into the CA1. *In vivo* two-photon calcium imaging was performed 21 days later. As for *in vivo* Ca²⁺ fiber photometry, optic fiber with ceramic ferrule (diameter: 2.5 mm, ThinkerTech, China) was implanted in the ipsilateral CA1 3 weeks after virus injection, and the calcium imaging and behavioral test were performed 7 days later. For the conditional knockout or knockdown experiments, 200 nl of AAV2/9-hSyn-Cre-EGFP-WPRE-pA (viral titer, 1.87 × 10¹³ genome copies/ml; Taitool Bioscience, China) or AAV2/9-U6-shRNA (*Celsr2*)-CMV-EGFP-pA (viral titer, 5.72 × 10¹² genome copies/ml; Brain VTA) was bilaterally injected into the CA1. For the DREADDs activation behavioral experiments, 200 nl of AAV2/9-CaMKIIα-hM3D(Gq)-EGFP-WPRE-hGH pA (viral titer, 3.10 × 10¹² genome copies/ml; Brain VTA) was bilaterally injected into the CA1.

In vivo Ca²⁺ fiber photometry

A commercialized fiber photometry system (ThinkerTech Inc.) was used to record the Ca²⁺ signals from the dorsal hippocampal CA1. Optic fiber with ceramic ferrule (diameter: 2.5 mm, ThinkerTech, China) was implanted in the ipsilateral CA1 (AP: 2.00 mm; ML: 1.80 mm; DV: 1.50 mm) 3 weeks after GCaMP6m virus injection. We used a skull-penetrating M1 screw and dental acrylic to support the ceramic ferrule. And the calcium imaging and behavioral test were performed 7 days later. The fluorescence signals were normalized within each mouse by calculating the delta fluorescence/fluorescence ($\Delta F/F_0$) as $(F - F_0)/F_0$, where F_0 is the baseline fluorescence signal averaged before the onset of the behavioral event. All animals used in the *in vivo* recording experiments were perfused after recording, and the positions of the recording sites were verified.

In vivo two-photon calcium imaging

As for *in vivo* calcium recording, the head skin and skull covering hippocampus were removed to create an imaging window (2 mm by 2 mm), which was covered by a glass coverslip. The calcium activities of CA1 somas were recorded at 2 Hz with a water-immersed objective (20x; ZEISS) during a 5 min period under an LSM780 two-photon microscope (ZEISS, Germany).

Acquired time series images were corrected by TurboReg module of ImageJ. The fluorescent value F was quantified by average pixels extracted from designed region of interest covering identifiable soma. The $\Delta F/F_0$ was calculated as $(F - F_0)/F_0$, where the F_0 was averaged F values during the first 10% recording period as the basal level. A calcium transient was defined when the $\Delta F/F_0$ is higher than threefold SDs.

Sparse labeling of neurons for studies of dendrites

To sparsely label pyramidal neurons in the hippocampus CA1, we used a new method based on *Nestin-CreER*^{T2} and *Rosa26*^{Tom} mice. *Nestin-CreER*^{T2} males were crossed with *Rosa26*^{Tom} females. Then a low dose (10 mg/kg) of tamoxifen (Sigma, T5648) was intraperitoneally injected into pregnant mice on E12.5 to induce the Cre enzyme to be randomly induced in a small part of neural precursor cells in the offspring. Tamoxifen was prepared by dissolving 10 mg powder in 1 ml preheated corn oil (Sigma, C8267) for a final concentration of 10 mg/ml. The mixture was placed in a 37 °C water bath and shaken for 2 h to dissolve completely, and then it was sealed in dark at 4 °C.

Analyses of dendrites and spines

For analysis of the CA1 region dendrites and spines, coronal 150 μ m vibratome sections were prepared from age-matched WT and *Celsr2* KO mice. Slides were individually coded and randomly ordered for image acquisition. Images of dendrites were acquired on Zeiss LSM 700 confocal microscope with a 20x lens. Images of the 2nd segment apical dendrite spine were acquired on LSM 700 confocal microscope with 63x lens and 2x optical zoom. The investigator was blind to genotype during image acquisition and analysis of dendritic and spine morphology. For dendritic analysis, both apical and basal processes of CA1 pyramidal neuron were analyzed. Three-dimensional (3D) reconstructions of the entire dendritic processes of each tdTomato⁺ neuron were obtained from Z-series stacks of confocal images using 3-D Imaris software. All tdTomato⁺ CA1 neurons with largely intact dendritic trees were analyzed for total dendritic length and branching. For complete 3D reconstruction of spines, consecutive stacks of images were acquired using an excitation wavelength of 488 nm at high magnification to capture the full depth of dendritic fragments

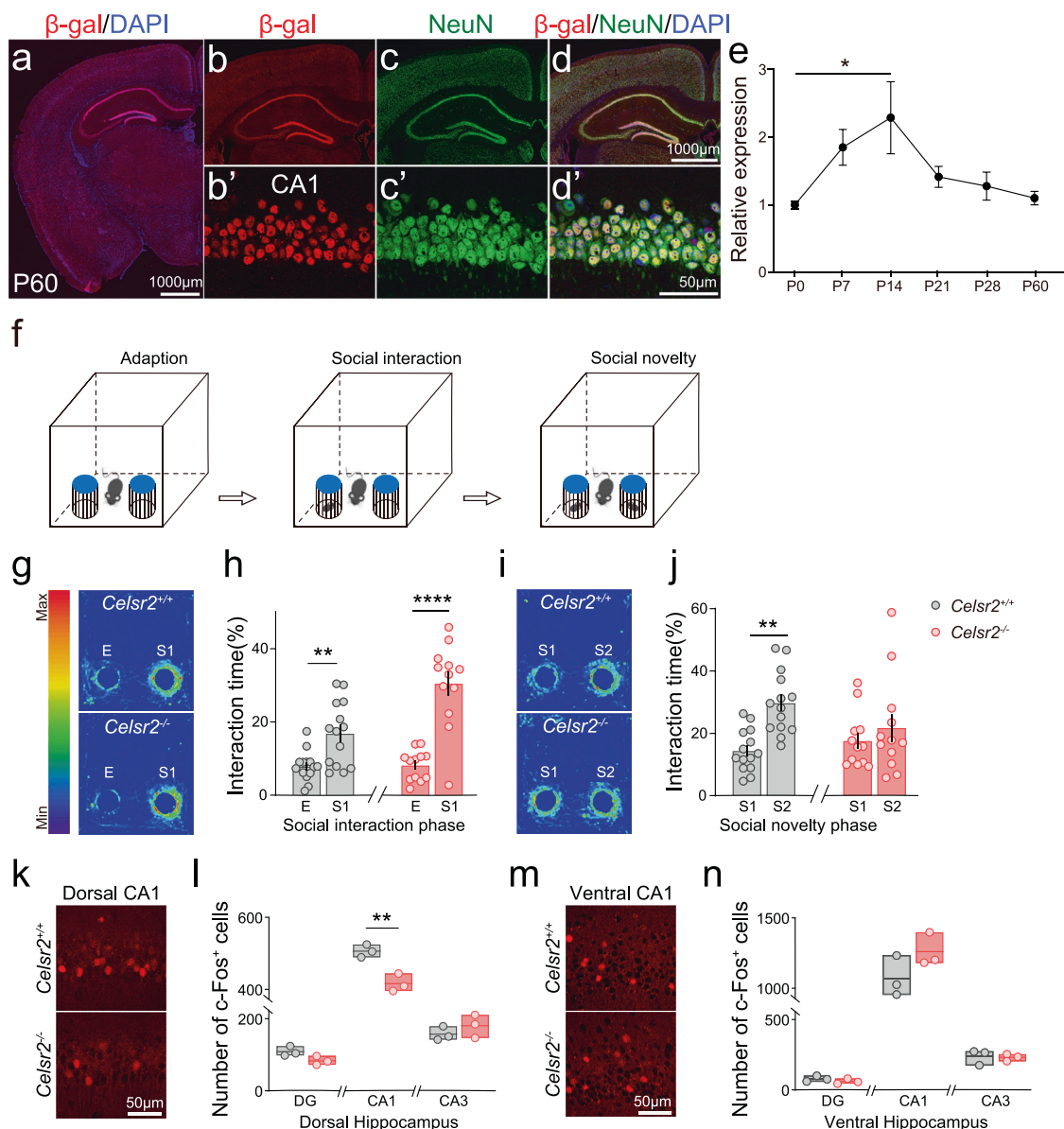


Fig. 1 *Celsr2* deficiency impairs social memory. **a** Low-magnification image showing the expression of Celsr2 detected by beta-galactosidase (red) immunohistochemistry in *Celsr2^{lacZ/+}* mice. Scale bar, 1000 µm. **b-d'** Fluorescence and immunohistochemistry double staining shows that Celsr2 (red) colocalizes with NeuN (to label neuronal nuclei) (green). **b, c, d** Hippocampal immunostaining for Celsr2 (red) indicates predominant expression in CA1 and DG region and modest expression in CA3. Scale bar, 1000 µm. **b', c', d'** Higher power images show most Celsr2 (red) in neurons (green) in CA1. Scale bar, 50 µm. **e** Quantitation of Celsr2 relative expression in hippocampus in P0, P7, P14, P21, P28, and P60 by quantitative PCR ($n = 4$ mice at every stage). Note the peak level at 2 weeks. **f** Protocol to test for social interaction and social novelty. Each phase lasts for 5 minutes. **g, h** Representative heat map images and summary data of time spent sniffing the empty cage (E) and the stranger 1 mouse (S1) during the social interaction phase (two-tailed paired *t*-test). **i, j** Representative heat map images and summary data of time spent sniffing the S1 and S2 during the social novelty phase (g-j: *Celsr2^{+/+}*: $n = 14$ mice; *Celsr2^{-/-}*: $n = 12$ mice; two-tailed paired *t*-test). Representative images of c-Fos activity in dorsal (**k**) and ventral (**m**) hippocampal CA1. Scale bar, 50 µm. Summary data of c-Fos activity in regions of dorsal (**l**) and ventral (**n**) hippocampus (*Celsr2^{+/+}*: $n = 3$ mice; *Celsr2^{-/-}*: $n = 3$ mice; two-tailed unpaired *t*-test). * $p < 0.05$; ** $p < 0.01$; **** $p < 0.0001$.

(20–50 µm long) and spines. The structure of dendritic fragments and spines was also traced using Imaris software.

Rescue experiments

For the NMDAR modulator treatment experiments, *Celsr2* KO mice were randomly intraperitoneally injected with DCS (Selleck.cn, S1998, in saline) at 20 mg/kg or with vehicle. Behavioral tests were performed 90 min after treatment. For chemogenetic manipulation, CNO (Target Mol., T4494, in saline) was administered 2 weeks after AAV2/9-CaMKIIa-hM3D(Gq)-EGFP-WPRE-hGh pA injection. These test mice were randomly intraperitoneally injected with CNO at 2 mg/kg or with vehicle. And behavioral tests were performed 30 min after treatment.

Statistical analysis

All data were presented as means \pm SEM. No data were excluded from this study. Data were firstly tested for normality. Two-sample student's *t*-test, one-way analysis of variance (ANOVA), and Tukey post hoc test were used to compare differences among two or multiple groups, respectively. For two independent variables, two-way ANOVA and Bonferroni post hoc comparison were adopted. A significant level was defined when $p < 0.05$. All statistical analysis was performed by GraphPad Prism 8.2 (La Jolla, CA, USA). All behavioral tests, dendrites and spines analyses, western blotting experiments and electrophysiology experiments were performed and analyzed by persons blinded to the grouping.

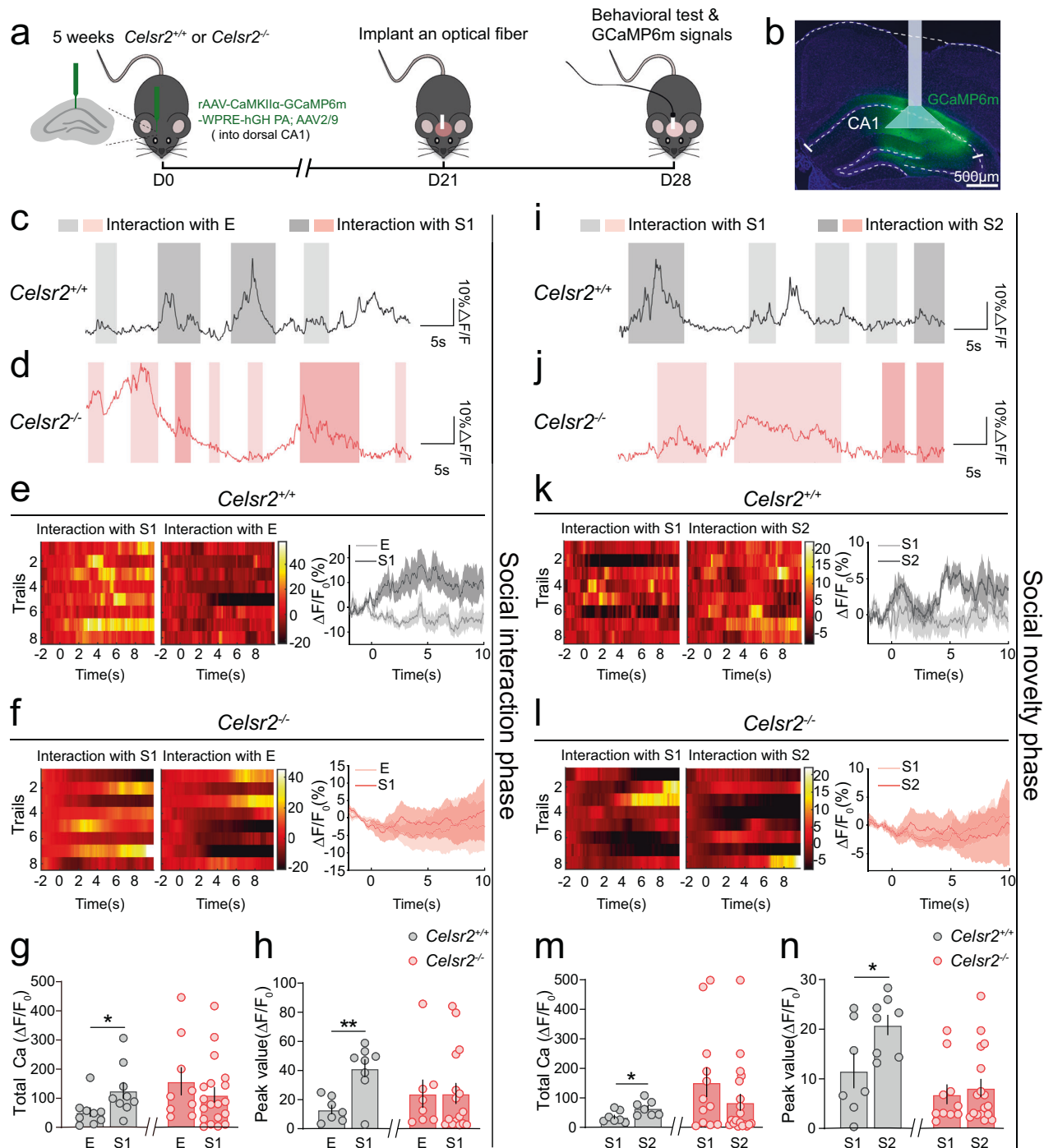
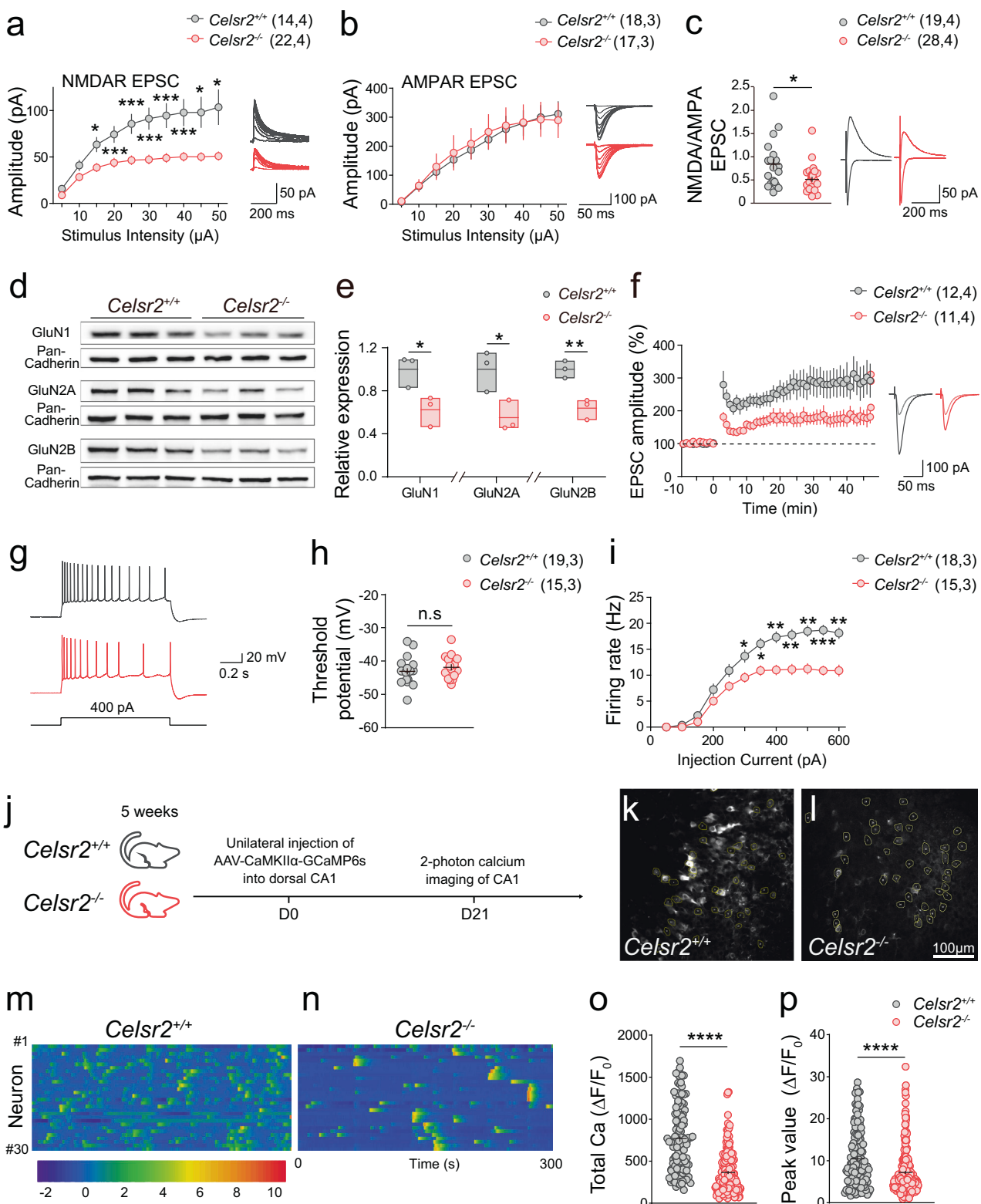


Fig. 2 *Celsr2* deficiency results in reduced CA1 pyramidal neuron activity during social tasks. **a** Schematic of the procedure used to record real-time calcium dynamics by fiber photometry recording implanted on *Celsr2*^{-/-} and *Celsr2*^{+/+} mice with AAV mediated GCaMP6m expression in CA1. **b** GCaMP6m virus injection site (green) and optic fiber placement. Scale bar, 500 μ m. **c-h** In *Celsr2*^{+/+} mice, CA1 neuronal activity was higher with stranger (S1) interaction when compared to empty cage (E), which was not detected in *Celsr2*^{-/-} mice. Representative tracts of calcium signaling activity in *Celsr2*^{+/+} (**c**) and *Celsr2*^{-/-} mice (**d**). **e, f** Heat maps illustrating the calcium response ($\Delta F/F_0$, %) of CA1 pyramidal neurons and peri-event plots of averaged calcium signals (*Celsr2*^{+/+}: $n = 8$ trials from 4 mice; *Celsr2*^{-/-}: $n = 8$ trials from 4 mice). **g, h** Summary plots of total integrated Ca^{2+} ($\Delta F/F_0$, %) and peak value of Ca^{2+} spikes ($\Delta F/F_0$, %) (two-tailed unpaired t-test). **i-n** During social novelty phase, neuronal activity was also higher when *Celsr2*^{+/+} mice met a new stranger (S2) compared to a familiar mouse (S1), which was not detected in *Celsr2*^{-/-} mice. Representative tracts of calcium signaling activity in *Celsr2*^{+/+} (**i**) and *Celsr2*^{-/-} mice (**j**). **k, l** Heat maps illustrating the calcium response ($\Delta F/F_0$, %) of CA1 pyramidal neurons and peri-event plots of averaged calcium signals (*Celsr2*^{+/+}: $n = 8$ trials from 4 mice; *Celsr2*^{-/-}: $n = 8$ trials from 4 mice). **m, n** Summary plots of total integrated Ca^{2+} ($\Delta F/F_0$, %) and peak value of Ca^{2+} spikes ($\Delta F/F_0$, %) (two-tailed unpaired t-test). Data are presented as the mean \pm SEM. * $p < 0.05$; ** $p < 0.01$.



RESULTS

Celsr2 deficiency results in impaired social memory

To study the expression of Celsr2 in adult mice, we used a Celsr2 allele in which beta-galactosidase (β -gal) is encoded by the gentrap construct [10], so that β -gal staining reflects Celsr2 expression. We checked expression at different stages, from

postnatal day 0 (P0) to adult (P60). Celsr2 expression was high in adult hippocampus, and present in almost all neurons (Fig. 1a-d). Expression increased after birth and persisted into adulthood (Supplementary Fig. 1), which was confirmed by RT-PCR, with mRNA peak levels at 2 weeks (Fig. 1e). We co-labelled hippocampal neurons with Neurogranin (NG) and GABA markers

Fig. 3 Celsr2 deficiency induces the dysfunction of NMDAR and impairment of synaptic plasticity in dCA1. **a–c** *Celsr2* deficiency resulted in reduced NMDAR-EPSCs (45–50% decrease) at strongest stimulation relative to *Celsr2*^{+/+}; 14 cells from 4 *Celsr2*^{+/+} mice; 22 cells from 4 *Celsr2*^{-/-} mice; two-way ANOVA with Bonferroni post tests. $F = 95.28$, $*p < 0.05$, $***p < 0.001$. **a** but not AMPAR-EPSCs (18 cells from 3 *Celsr2*^{+/+} mice; 17 cells from 3 *Celsr2*^{-/-} mice; two-way ANOVA with Bonferroni post tests. $F = 0.1657$, $p > 0.05$, **b**) together with reduced NMDA/AMPA ratio (19 cells from 4 *Celsr2*^{+/+} mice; 28 cells from 4 *Celsr2*^{-/-} mice; unpaired t test, $*p = 0.020752075$, **c**). Representative traces are shown in the right panel of each graph. **d, e** Membrane protein levels of glutamate receptor subunits GluN1, GluN2A and GluN2B were reduced in hippocampus from *Celsr2*^{-/-} mice. Pan-Cadherin was used as a loading control (**d**). Quantitative analyses of integral density signal were normalized to the Ctrl levels (two-tailed unpaired t -test) (**e**). **f** Time-course changes of EPSC amplitude (% of baseline) after a pairing protocol (0 mV, 2 Hz, 360 pulses) measured from *Celsr2*^{+/+} (12 cells, 4 mice) and *Celsr2*^{-/-} (11 cells, 4 mice) groups (*Celsr2*^{+/+}: 288.84 ± 35.84 ; *Celsr2*^{-/-}: 187.59 ± 22.58 , $*p = 0.0126$, two-tailed unpaired t -test). Representative traces before and at 30–40 min after pairing are shown on the right. Representative traces of action potential (**g**) from *Celsr2*^{+/+} and *Celsr2*^{-/-} mice by current injection at 400 pA, the threshold potential (**h**) of both mice (*Celsr2*^{+/+}, -43.10 ± 0.94 mV, 19 cells, 3 mice; *Celsr2*^{-/-}: -41.89 ± 0.93 mV, 15 cells, 3 mice, $p = 0.3756$, two-tailed unpaired t -test) and averaged firing rates (**i**) of CA1 pyramid neurons from *Celsr2*^{+/+} (18 cells, 3 mice) and *Celsr2*^{-/-} (15 cells, 3 mice) groups, induced by 50 pA step-current injections (0–600 pA; two-way ANOVA with Bonferroni post tests. $F = 116.0$, $*p < 0.05$, $**p < 0.01$, $***p < 0.001$). **j** Schematic of the procedure of 2-photon microscopy imaging of calcium dynamics of CA1 pyramidal neurons *in vivo*. Representative images of calcium fluorescence obtained from somas of CA1 during a 5 min period in *Celsr2*^{+/+} (**k**) and *Celsr2*^{-/-} (**l**) mice. **m, n** Representative heat maps illustrating the calcium response ($\Delta F/F_0$, %) of CA1 pyramidal neurons. (*Celsr2*^{+/+}: $n = 30$ neurons from 1 mouse; *Celsr2*^{-/-}: $n = 30$ neurons from 1 mouse). Summary plots of total integrated Ca^{2+} ($\Delta F/F_0$, %) (**o**) and peak value of Ca^{2+} spikes ($\Delta F/F_0$, %) (**p**). The results demonstrated reduced CA1 neuronal activity *in vivo* in *Celsr2*^{-/-} mice (*Celsr2*^{+/+}: $n = 183$ neurons from 3 mice; *Celsr2*^{-/-}: $n = 195$ neurons from 3 mice; two-tailed unpaired t -test). $*p < 0.05$; $**p < 0.01$; $***p < 0.001$; $****p < 0.0001$.

of excitatory and inhibitory neurons, respectively. We found that *Celsr2* was mainly expressed in excitatory pyramidal neurons (Supplementary Fig. 2).

In open field, novel object recognition, Y-maze, and grooming tests, *Celsr2* KO (*Celsr2*^{-/-} mice) showed normal locomotor activity, normal memory for a novel object, normal working memory, and grooming behavior (Supplementary Fig. 3a–f). To evaluate whether *Celsr2* regulates social memory, we tested for sociability and social memory under free-choice conditions (Fig. 1f). Sociability can be determined by the preference for a cage containing a stranger mouse (S1) versus an empty cage (E) during the social interaction phase. Like control (*Celsr2*^{+/+}) mice, *Celsr2* KO mice spent more time interacting with the stranger mouse than with the empty cage, indicating that *Celsr2*^{-/-} mice have normal sociability (Fig. 1g, h). In the test for mice to distinguish between a stranger mouse and a novel object, *Celsr2*^{-/-} mice also showed similar sociability as control mice (Supplementary Fig. 3g). Social memory was quantified by measuring the interaction time that a test mouse spent with a novel stranger mouse (S2) versus a familiar mouse (S1) during the social novelty phase. Mice naturally prefer to spend more time interacting with a novel conspecific, and indeed wild-type control mice spent more time interacting with S2 than S1 (Fig. 1i, j). In contrast, when facing a newly introduced unfamiliar conspecific, unlike *Celsr2*^{+/+} mice, *Celsr2*^{-/-} mice failed to distinguish between the two choices (Fig. 1i, j), indicating selective impairment in social memory.

To identify the brain regions responsible for this behavioral defect, we performed c-Fos mapping following the social behavior paradigm. Notably, there was a selective reduction in the number of c-Fos positive (c-Fos⁺) cells in dorsal CA1 region, but not in ventral CA1, Dentate Gyrus, and CA3 regions (Fig. 1k–n) in *Celsr2* KO mice compared to control mice. These results indicate that *Celsr2* may affect hippocampal circuitry to regulate social memory.

***Celsr2* deficiency results in reduced CA1 pyramidal neuron activity during social tasks**

To study real-time hippocampal neuron activity during social tasks, we transfected GCaMP6m into hippocampal dorsal CA1 (dCA1) pyramidal neurons and implanted optic fibers for fiber photometry recording in *Celsr2*^{+/+} and *Celsr2*^{-/-} mice (Fig. 2a, b). In the sociability test, the dCA1 neurons of *Celsr2*^{+/+} mice became significantly activated in the S1 compared to E situation, but no differences between S1 and E conditions were detected in *Celsr2*^{-/-} mice (Fig. 2c–h). In social memory tests, dCA1 neuronal activity was also increased when *Celsr2*^{+/+} mice met a new stranger (S2), compared to meeting a familiar partner (S1). In contrast, no such difference was found when *Celsr2*^{-/-} mice interacted with S1 or S2

partners (Fig. 2i–n). These results show that *Celsr2* deficiency results in reduced dCA1 neuronal activity during social tasks.

***Celsr2* deficiency reduces NMDAR function and impairs synaptic plasticity in dCA1**

We examined synaptic transmission and neuronal excitability of dCA1 neurons in *Celsr2* KO and control mice by ex vivo electrophysiological recordings. To study synaptic transmission in hippocampus, we firstly compared NMDAR and α -amino-3-hydroxy-5-methylisoxazole-4-propionic acid receptor (AMPAR) mediated excitatory postsynaptic currents using whole-cell recording from dCA1 pyramidal neurons. We found that *Celsr2* deficiency resulted in significantly smaller NMDAR-mediated EPSCs amplitudes in mutant than in control neurons, without affecting AMPAR-mediated EPSCs amplitudes (Fig. 3a, b). Accordingly, NMDA/AMPA ratio was reduced in *Celsr2* KO versus control mice (Fig. 3c). The amplitude of miniature excitatory synaptic currents (mEPSCs) was a smaller in *Celsr2* KO mice than in control mice (Supplementary Fig. 4a–c), whereas miniature inhibitory synaptic currents (mIPSCs) were unchanged (Supplementary Fig. 4d–f). We then confirmed the reduction in the different subunits of NMDARs using western blotting analysis of membrane components from hippocampus in *Celsr2* KO mice (Fig. 3d, e), showing the same trend as the results from total lysate of hippocampus (Supplementary Fig. 5). The synaptic composition of NMDAR subunits was examined by isolating NMDAR-EPSCs blocked by the GluN2B antagonist ifenprodil (3 μ M); the inhibition of NMDAR-EPSCs by ifenprodil was significantly weaker in *Celsr2* KO than in control neurons, suggesting that *Celsr2* KO neurons contain less synaptic GluN2B-containing receptors (Supplementary Fig. 4g). Moreover, the reduced NMDAR function was accompanied with impaired Schaffer collaterals (SC) to CA1 pathway LTP in *Celsr2*^{-/-} mice (Fig. 3f).

Using current injection, we found that dorsal CA1 neurons from *Celsr2* KO mice were less excitable than those in control mice (Fig. 3g–i). To confirm the *in vivo* relevance of our brain slice findings, we recorded calcium activities in dorsal CA1 pyramidal neurons in awake mice. *In vivo* 2-photon calcium imaging was performed after transfecting the genetically encoded calcium indicator GCaMP6s into hippocampal dorsal CA1 pyramidal neurons (Fig. 3j), and calcium transients in CA1 neurons were recorded in head-fixed, awake *Celsr2*^{+/+} and *Celsr2*^{-/-} mice (Fig. 3k, l). In line with the results from brain slice recording, *Celsr2* KO mice displayed reduced levels of spontaneous calcium activities, and smaller peak value of calcium spikes (Fig. 3m–p). In sum, the absence of *Celsr2* results in impaired synaptic transmission and plasticity, as well as hypoactivity in dorsal hippocampus.

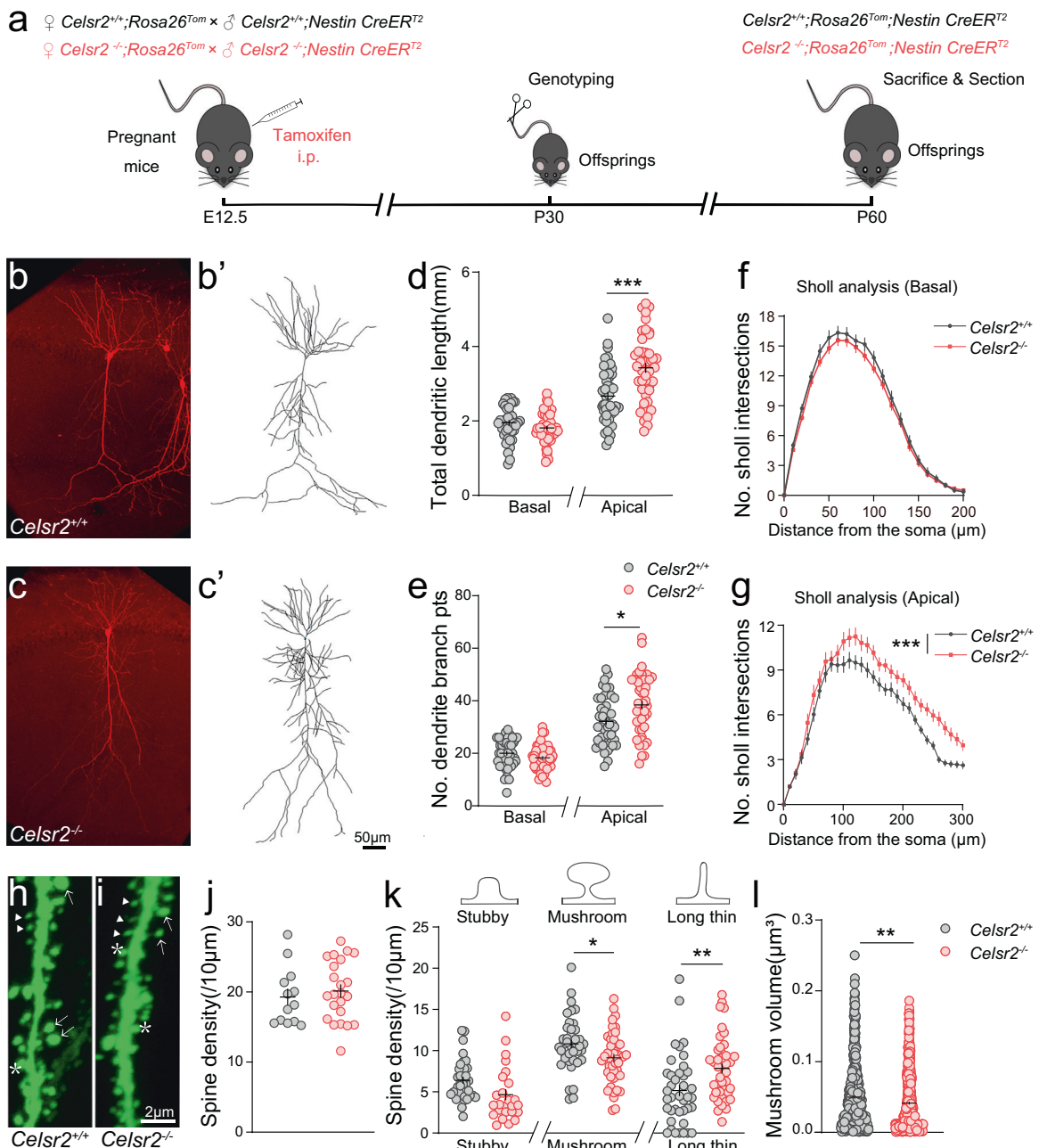
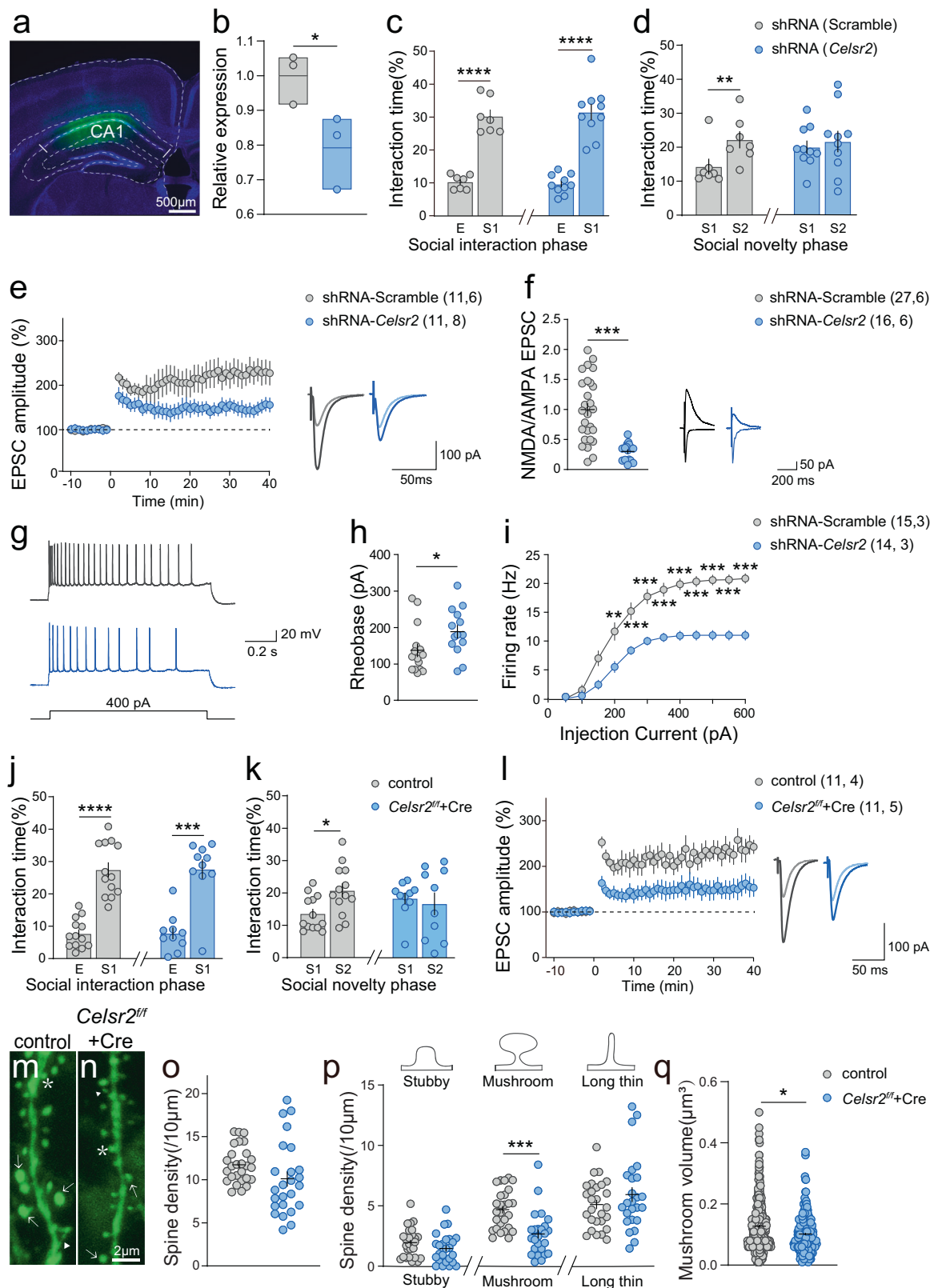


Fig. 4 *Celsr2* deficiency leads to exuberant dendrite formation in vivo. **a** Schematic of the procedure used to sparsely label CA1 pyramidal neurons. **b–c'** Representative confocal projection images (**b**, **c**) and three-dimensional reconstruction images (**b'**, **c'**) of tdTomato-labelled pyramidal neurons from the CA1 region of hippocampus in *Celsr2^{+/+}* (**b**, **b'**) and *Celsr2^{-/-}* (**c**, **c'**) mice. Scale bar, 50 μm. **d–g** Summary plots of total dendrite length (**d**, two-tailed unpaired t-test) and branch numbers (**e**, two-tailed unpaired t-test). Sholl analysis of basal (**f**) and apical (**g**) dendrite arbors in neurons from *Celsr2^{+/+}* and *Celsr2^{-/-}* mice. *Celsr2* deficiency resulted in increased length and branch numbers of the apical but not basal dendrites; Sholl analysis confirmed the exuberant apical dendrite arbors in neurons from *Celsr2^{-/-}* mice (Basal: $n = 42$ dendrites from 11 *Celsr2^{+/+}* mice and $n = 49$ dendrites from 14 *Celsr2^{-/-}* mice. Apical: $n = 45$ dendrites from 11 *Celsr2^{+/+}* mice and $n = 45$ dendrites from 14 *Celsr2^{-/-}* mice; two-way ANOVA with Bonferroni's multiple comparisons test). Representative confocal stack images of Thy1-labelled CA1 pyramidal neuronal apical dendrites and spines in *Celsr2^{+/+}* (**h**) and *Celsr2^{-/-}* (**i**) mice. Spine types: asterisk for stubby, arrows for mushroom, arrowheads for long thin. Scale bar, 2 μm. Summary plots of spine density (**j**), spine types (**k**) and volume of mature spine (mushroom) (**l**) on the secondary apical dendrites. *Celsr2* deficiency did not result in alteration in total number of spines, but the density and volume of mature spine (mushroom) were significantly reduced (*Celsr2^{+/+}*: $n = 20$ dendrites from 5 mice; *Celsr2^{-/-}*: $n = 23$ dendrites from 6 mice; two-tailed unpaired t-test). * $p < 0.05$; ** $p < 0.01$; *** $p < 0.001$.

Celsr2 deficiency affects CA1 pyramidal cell dendritic homeostasis in vitro and in vivo

Neurons adjust their dendritic growth and branching to compensate for changes in activity and synaptic input, which is referred to as structural homeostasis [26, 27]. Previous reports documented the

activity- and NMDA receptor-dependent formation and pruning of dendritic arbors of CA1 pyramidal neurons [28]. This prompted us to examine morphological changes of CA1 neurons in *Celsr2* KO animals. The hippocampal cytoarchitecture of *Celsr2* KO mice was unremarkable, and CTB labeling revealed no changes in



hippocampal axon projection (Supplementary Figs. 6 and 7). In isolated hippocampal neurons, neuronal dendrites were identified by anti-Map2 staining (Supplementary Fig. 8a–p). Cultured *Celsr2*^{−/−} neurons initially exhibited reduced dendrite complexity compared to *Celsr2*^{+/+} neurons (3 days in vitro, DIV 3, Supplementary

Fig. 8a–d), but then the dendrites of *Celsr2*^{−/−} neurons grew more extensively than control ones (Supplementary Fig. 8e–l). At DIV 12, the number and total length of dendrites were increased in *Celsr2*^{−/−} compared to *Celsr2*^{+/+} neurons (Supplementary Fig. 8m–p). To study the dynamics of dendrite growth, we carried

Fig. 5 Celsr2 knockdown in adulthood recapitulates social memory and spine deficits. **a** Injection site (green) of AAV-Celsr2 or scramble shRNA into the dorsal CA1 of adult WT mice. Scale bar, 500 μ m. **b** Quantitation of Celsr2 relative expression by quantitative PCR ($n = 3$ mice per group). **c, d** Celsr2 knockdown led to social memory deficits. Summary data of time spent sniffing the empty cage (**c**) and the stranger 1 mouse (**d**) at the social interaction phase (**c**) and time spent sniffing the S1 and the S2 at the social novelty phase (**d**) (control: $n = 7$ mice; knockdown: $n = 10$ mice; two-tailed paired t-test). **e** Time-course changes of EPSC amplitude (% of baseline) after a pairing protocol (0 mV, 2 Hz, 360 pulses) measured in control (228.37 ± 27.47 , 11 cells, 6 mice) and Celsr2 knockdown mice (147.88 ± 14.5 , 11 cells, 8 mice) groups ($^{*}p = 0.0292$, two-tailed unpaired t-test). Representative traces before and at 30–40 min after pairing are shown on the right. **f** NMDAR-EPSC to AMPAR-EPSC ratios from control mice and Celsr2 knockdown mice (control: 0.998 ± 0.179 , 27 cells, 6 mice; knockdown: 0.301 ± 0.037 , 16 cells, 6 mice; unpaired t-test, $^{***}p < 0.001$). Representative traces are shown on the right. **g–i** Representative traces of action potential from control mice and Celsr2 knockdown mice by current injection at 400 pA (**g**, control: black and knockdown: blue). The rheobase of action potential (minimum pA required for initiating an action-potential) increased in knockdown cells (**h**, control: 132.66 ± 17.12 pA, 15 cells, 3 mice; knockdown: 183.57 ± 17.24 pA, 14 cells, 3 mice, $^{*}p < 0.05$, unpaired t-test) and averaged firing rate of CA1 pyramidal neurons from control (15 cells, 3 mice) and knockdown (14 cells, 3 mice) cells, induced by 50 pA step-current injections (**i**, 0–600 pA; two-way ANOVA with Bonferroni post-tests. $F = 45.58$, $^{**}p < 0.01$, $^{***}p < 0.001$). **j–l** Conditional Celsr2 knockout (*Celsr2^{ff} + Cre*) by injecting AAV-Cre in CA1 region of *Celsr2^{ff}* adult mice. The results were comparable to *Celsr2* KO and Celsr2 knockdown, showing social memory deficits, together with reduced CA1 LTP. Summary data of time spent sniffing the empty cage (**j**) and the stranger 1 mouse (**k**) at the social interaction phase (**j**) and time spent sniffing the S1 and the S2 at the social novelty phase (**k**) (control: $n = 13$ mice; *Celsr2^{ff} + Cre*: $n = 10$ mice; two-tailed paired t-test). Time-course changes of EPSC amplitude (% of baseline) after a pairing protocol (0 mV, 2 Hz, 360 pulses) measured in control (253.31 ± 23.55 , 11 cells, 4 mice) and *Celsr2^{ff} + Cre* mice (153.12 ± 18.84 , 11 cells, 5 mice) groups (**l**, two-tailed unpaired t-test, $^{**}p = 0.0036$). Representative traces before and at 30–40 min after pairing are shown on the right. Representative confocal stack images of YFP-labelled CA1 pyramidal neuronal apical dendrites and spines in control (**m**) and *Celsr2^{ff} + Cre* (**n**) neurons. Spine types: asterisk for stubby, arrows for mushroom, arrowheads for long thin. Scale bar, 2 μ m. Summary plots of spine density (**o**), spine types (**p**), and volume of mature spine (mushroom) (**q**) on the secondary apical dendrites. (Control: $n = 27$ dendrites from 3 mice; *Celsr2^{ff} + Cre*: $n = 25$ dendrites from the same 3 mice; two-tailed unpaired t-test). $^{*}p < 0.05$; $^{**}p < 0.01$; $^{***}p < 0.001$; $^{****}p < 0.0001$.

out live-time imaging of cultured neurons, and found increased extension and reduced retraction of dendritic branches in *Celsr2*^{-/-} neurons (Supplementary Fig. 8q–s), accounting for the overgrowth of dendrites in *Celsr2* mutants. Notably, dendritic overgrowth was associated with impaired excitatory synapses development, as revealed by reduced staining of vesicular glutamate transporter 1 (VGluT1) and PSD-95 positive clusters (Supplementary Fig. 8t–v).

We then studied dendrite development *in vivo*, using a new method for sparse labeling of CA1 pyramidal neurons. *Celsr2*^{+/+}; *Rosa26^{Tom};Nestin-CreER^{T2}* and *Celsr2*^{-/-}; *Rosa26^{Tom};Nestin-CreER^{T2}* mice were injected with a low dose of tamoxifen at E12.5 to induce sparse neurons to express tdTomato, and the dendritic morphology of sparsely labeled CA1 pyramidal neurons was analyzed at P60 (Fig. 4a). We found that *Celsr2* deficiency resulted in increased total dendritic length and branch numbers of apical but not basal dendrites (Fig. 4b–e). Sholl analysis confirmed the exuberant apical dendrite arbors in CA1 neurons from *Celsr2*^{-/-} mice (Fig. 4f, g). To assess whether *Celsr2* acts cell autonomously or not, we inactivated *Celsr2* specifically in sparsely labeled neurons using *Celsr2*^{-/-}; *Rosa26^{Tom};Nestin-CreER^{T2}*. The results indicated that the function of *Celsr2* was partly cell-autonomous (Supplementary Fig. 9).

To examine dendritic spines, we used *Celsr2*^{+/+}; *Thy1-YFP* and *Celsr2*^{-/-}; *Thy1-YFP* mice. *Celsr2* deficiency did not result in any modification of total spine densities in apical dendrites of CA1 pyramidal neurons (Fig. 4h–j). However, the density and volume of mature (mushroom) spines were significantly reduced in *Celsr2* mutant neurons, and this was accompanied with a proportional increase in the number of immature, long thin spines (Fig. 4k, l). Thus, deficiency of *Celsr2* leads to exuberant apical dendrites and immaturity of spines in CA1 pyramidal neurons.

The homeostatic roles of *Celsr2* in adult hippocampus

Considering the persistent expression of *Celsr2* in the adult, a critical question is whether *Celsr2* affects social memory through direct regulation of adult synaptic functions. To address that question, we selectively knocked down *Celsr2* in adult CA1 by injecting AAV2/9-shRNA (*Celsr2*) to the dorsal CA1 of adult WT mice, and verified by RT-PCR that *Celsr2* expression was nearly abrogated in CA1 (Fig. 5a, b). The manipulation did not alter natural sociability (Fig. 5c), but produced deficits in social memory (Fig. 5d), similar to those observed in *Celsr2* KO mice. Whole-cell recordings revealed changes similar to that in mutant mice,

including impaired CA1 LTP and reduced NMDAR/AMPAR ratio (Fig. 5e, f). The excitability of dCA1 pyramidal neurons from *Celsr2* knockdown mice was less than those from control mice (Fig. 5g–i), similar to the dCA1 neurons from *Celsr2* KO mice.

In addition to shRNA knockdown, we inactivated *Celsr2* by injecting AAV-Cre in the CA1 region of *Celsr2^{ff}* adult mice. Results were comparable to those in *Celsr2* KO or upon *Celsr2* shRNA knockdown, namely a social deficit selectively in social novelty phase (Fig. 5j, k), together with reduced CA1 LTP (Fig. 5l). To investigate whether *Celsr2* knockdown in adult could affect spine structure, we injected low concentration AAV2/9-hSyn-CremCherry to one side of hippocampus in *Celsr2^{ff};Thy1-YFP* mice. *Celsr2* was specifically deleted in red fluorescent neurons, and we analyzed the spines of red fluorescent neurons which were co-labeled by Thy1-YFP, the green fluorescent-only neurons in the contralateral side serving as controls (Supplementary Fig. 10). Similar to results observed in *Celsr2* KO mice, selective deletion of *Celsr2* in adult CA1 pyramidal neuron did not affect spine density (Fig. 5m–o), but led to reduced density and volume of mature (mushroom) spines (Fig. 5p, q). These findings support the importance of *Celsr2* in normal adult NMDAR function and social behavior.

Potentiating NMDAR function or CA1 neuronal activity rescues social memory impairment in *Celsr2* deficient mice

If defective NMDAR function is a major cause of hypoactivity in *Celsr2* KO mice, increasing NMDAR activity may improve their social memory. We injected saline or D-cycloserine (DCS), a partial NMDAR agonist, to *Celsr2*^{-/-} mice, and carried out social behavior tests 90 minutes later (Fig. 6a). *Celsr2*^{-/-} mice that received DCS spent more time interacting with S2 partners than saline group, showing the DCS application indeed improved their social memory (Fig. 6b, c).

Given that dorsal CA1 neuron hypoactivity was associated with social memory deficits in *Celsr2*^{-/-} mice, could the activation of dCA1 pyramidal neurons rescue social memory deficits? We address this, by using a chemogenetic strategy to modulate CA1 neuronal activity, by expressing Designer Receptors Exclusively Activated by Designer Drugs (DREADD). We injected AAV2/9-CaMKIIα-hM3D(Gq)-EGFP to dorsal CA1 in *Celsr2*^{-/-} mice. Two weeks later, the DREADD ligand clozapine N-oxide (CNO) (to activate CA1 transfected neurons) or saline (control) was injected intraperitoneally 30 minutes before behavioral tests (Fig. 6d). The

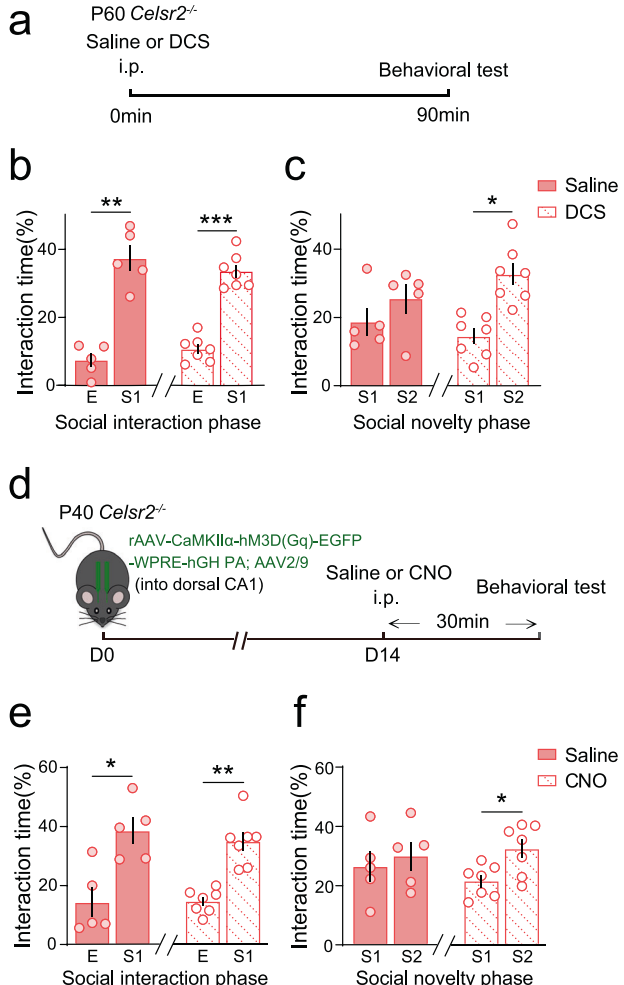


Fig. 6 Rescuing social deficits in *Celsr2* KO mice by enhancing NMDAR function or CA1 neuron activity. **a–c** Rapid restoration of social recognition ability in *Celsr2* KO mice by enhancing NMDAR function. **a** Schematic of the procedure for intraperitoneal injection of D-cycloserine (DCS), a partial agonist for NMDAR. **b, c** Summary data of time spent sniffing the empty cage (E) and the stranger 1 mouse (S1) at the social interaction phase (**b**) and time spent sniffing the S1 and S2 at the social novelty phase (**c**) (saline group: $n = 5$ mice; DCS group: $n = 7$ mice; two-tailed paired t -test). **d–f** Chemogenetic activation of CA1 pyramidal neurons rescued the social memory deficit in *Celsr2* KO mice. **d** Schematic of the procedure for chemogenetically manipulating neuronal activity by using AAV-CaMKIIα-hM3D(Gq)-EGFP injection into dorsal CA1. **e–f** Summary data of time spent sniffing the empty cage (E) and the stranger 1 mouse (S1) at the social interaction phase (**e**) and time spent sniffing the S1 and the S2 at the social novelty phase (**f**) (saline group: $n = 5$ mice; CNO group: $n = 7$ mice; two-tailed paired t -test). * $p < 0.05$; ** $p < 0.01$; *** $p < 0.001$.

results showed that chemogenetic activation of CA1 pyramidal neurons was able to rescue the social behavior deficit in *Celsr2* KO mice (Fig. 6e, f).

DISCUSSION

Our results show a previously unsuspected role of *Celsr2* in the formation of social memory. Social memory formation depends on the appropriate function of various brain regions, particularly on the hippocampus, on which our analysis was therefore focused. We show that *Celsr2* deficiency results in decreased dCA1 pyramidal neuron activity during social interaction, reduces NMDAR function, and impairs synaptic plasticity and dendritic homeostasis in CA1 pyramidal neurons, *in vitro* as well as *in vivo*. Similar defects were observed when *Celsr2* was inactivated in adult animals, and social memory impairments were rescued by potentiating NMDAR function or increasing CA1 neuronal activity. Our observations raise several questions, particularly about: (i) Intraneuronal signals relayed by *Celsr2* and their interactions with NMDAR signaling in social memory formation; (ii) the role of *Celsr2* in dendritic structural homeostasis and synaptic plasticity; and (iii) a putative

function of other molecules of the planar cell polarity (PCP) pathway in adult brain.

The atypical cadherin *Celsr* family is composed of three members *Celsr1–3*, among which only *Celsr2* is expressed in the adult brain, including the hippocampal formation. *Celsr2* harbors a large ectodomain that includes eight cadherin repeats, and belongs to the adhesion G-protein-coupled receptor family (hence its alternative name Adgrc2). A previous study in rat primary hippocampal neuron culture suggests that *Celsr2* can be activated by homophilic interactions and increases calcium activity [14]. Here, we show that *Celsr2* is strongly expressed in hippocampal formation and, using *in vivo* 2-photon calcium imaging and fiber photometry recording, we confirm that *Celsr2* deficiency leads to decreased neuronal calcium activity.

A first question concerns the relations between *Celsr2* and NMDAR function. Although the molecular mechanisms by which the hippocampus regulates the formation of social memory remain elusive, NMDAR function and associated changes in synaptic plasticity are recognized as important cellular factors [8, 29, 30]. It is therefore relevant that *Celsr2* deficiency specifically impairs NMDAR but not AMPAR transmission. A recent study from

our group showed that *Celsr2* downregulation resulted in increased activity of Rac1/Cdc42 and JNK/c-Jun pathways and impacted axon regeneration in adult [17]. Of note, independent studies showed that NMDAR could be regulated by Rac1. *Shank3-deficient* mice exhibit social deficits and diminished NMDAR synaptic function and distribution, and this is associated with blunted Rac1/PKA activity and reduced synaptic F-actin [31]. *Dock4* KO mice have impaired social memory and reduced NMDAR expression, which is caused by reduced Rac1 activity [32]. Therefore, *Celsr2* may regulate NMDAR distribution and function through cytoskeletal dynamics. It is also conceivable that decreased membrane trafficking of NMDARs in hippocampal neurons contributes to social memory deficits, as has been reported in *SorCS2-deficient* mice [8].

A second question is the role of *Celsr2* in structural homeostasis and synaptic plasticity. Using rat neuron and brain slice culture, previous work reported that *Celsr2* enhanced dendrite growth, and that *Celsr2* knockdown led to simplification of dendritic arbors [13, 14]. In contrast, we found overgrowth of apical dendrites in CA1 pyramidal neurons of *Celsr2* KO mice. An explanation for this apparent contradiction is provided by our observation that *Celsr2* mutant dendrites develop more slowly than their WT counterparts during the first few three days in vitro (up to DIV 3), and become exuberant later, at DIV 9 and even more at DIV 12, which is consistent with the dynamics of neuronal activity. In line with our results, in *Drosophila*, dendrite overgrowth was observed in mutants of *Flamingo*, the ortholog of *Celsr2* [33]. A possible explanation for this exuberant dendritic phenotype is that *Celsr2/Flamingo* deficiencies *in vivo* lead to reduced neuronal activity, and dendritic arbors adjust their growth to compensate for activity reduction, a phenomenon often referred to as structural homeostasis [26, 27]. In *Drosophila*, compensatory changes of dendritic arbor structure were observed in response to input variations, such as decreased presynaptic input resulting in overgrowth of postsynaptic dendritic arbor [26]. Neural activity mediated by postsynaptic NMDAR plays an important role in neural circuit formation and refinement [34–36]. Sensory input acting through NMDAR and Wnt5 signaling pathways are involved in dendritic refinement in *Drosophila*, with reduced activity also resulting in increased dendritic length [37]. Activity-dependent signals can limit the growth of dendrites; for example, inhibition of NMDAR or CaMKII activity increased the growth of tectal cell dendrites in *Xenopus* [38]. NMDAR blockade caused markedly increased dendritic branching of lateral geniculate nucleus (LGN) cells in ferrets [39]. Inhibition of NMDAR in hippocampal slice culture led to a more complex dendritic arborization of CA1 pyramidal neurons in rat [28]. It is therefore reasonable to propose that *Celsr2* deficiency leads to decreased NMDAR-mediated Ca^{2+} signaling and neuronal activity, and this affects dendrite structural homeostasis and results in exuberant dendrites.

A third question concerns the putative role of other planar cell polarity (PCP) signaling molecules. As stated above, *Celsr2* is a core component of PCP signaling pathways that play critical roles in regulating brain development, from neural progenitor cell fate decision, neural migration, axon guidance, to dendrite formation [9, 40]. Previous studies have shown that two other PCP members, *Vangl2* and *Prickle2*, are crucial for synaptogenesis [41]. *Vangl2* induces synapse formation through direct interaction with N-Cadherin and PSD-95 [41–44], whereas *Prickle2* interacts with PSD-95 and NMDAR and regulates formation of postsynaptic complexes [45]. *Prickle2* mutant mice have deficits in social interactions, and this is associated with reduced synapse number and decreased size of postsynaptic densities in hippocampus [46]. Other studies have shown that *Celsr3*, *Fzd3* and *Vangl2* were involved in glutamatergic synapse formation and maintenance [47, 48]. Unlike *Celsr3*, which is downregulated after birth [16], the expression of *Celsr2* increases after birth and persists into

adulthood, indicating that it may play more important roles than *Celsr3* in adult brains. Persistent expression of *Celsr2* maintains synapse morphology, regulates hippocampal NMDAR function and social memory integrity in adults, and could perform that role in collaboration with *Vangl2*, and possibly *Prickle2*.

Finally, our study was focused on the hippocampus because its role in social memory is widely accepted. However, social memory depends on the appropriate function of several other brain regions such as the medial prefrontal cortex, anterior cingulate cortex, and amygdala [1, 2], all of which express various levels of *Celsr2* and PCP genes. To understand and integrate the neuronal circuits that mediate the formation of social memory, further studies should address the role of *Celsr2* and other PCP genes in those brain regions.

Altogether, our work points to a key role of *Celsr2* to regulate social memory formation. *Celsr2* acts in interaction with NMDAR and neuronal activity in CA1. NMDARs and interacting partners such as *Celsr2* are potential therapeutic targets for the management of social deficit disorders, such as in autism.

REFERENCES

1. Tanimizu T, Kenney JW, Okano E, Kadoma K, Frankland PW, Kida S. Functional connectivity of multiple brain regions required for the consolidation of social recognition memory. *J Neurosci*. 2017;37:4103–16.
2. Guo B, Chen J, Chen Q, Ren K, Feng D, Mao H, et al. Anterior cingulate cortex dysfunction underlies social deficits in *Shank3* mutant mice. *Nat Neurosci*. 2019;22:1223–34.
3. Okuyama T, Kitamura T, Roy DS, Itohara S, Tonegawa S. Ventral CA1 neurons store social memory. *Science*. 2016;353:1536–41.
4. Chai AP, Chen XF, Xu XS, Zhang N, Li M, Li JN, et al. A temporal activity of CA1 neurons underlying short-term memory for social recognition altered in PTEN mouse models of autism spectrum disorder. *Front Cell Neurosci*. 2021;15:699315.
5. Sellami A, Al Abed AS, Brayda-Bruno L, Etchamendy N, Valerio S, Oule M, et al. Temporal binding function of dorsal CA1 is critical for declarative memory formation. *Proc Natl Acad Sci USA* 2017;114:10262–7.
6. Hitti FL, Siegelbaum SA. The hippocampal CA2 region is essential for social memory. *Nature*. 2014;508:88–92.
7. Watarai A, Tao K, Wang MY, Okuyama T. Distinct functions of ventral CA1 and dorsal CA2 in social memory. *Curr Opin Neurobiol*. 2021;68:29–35.
8. Yang J, Ma Q, Dincheva I, Giza J, Jing D, Marinic T, et al. *SorCS2* is required for social memory and trafficking of the NMDA receptor. *Mol Psychiatry*. 2021;26:927–40.
9. Tissir F, Goffinet AM. Shaping the nervous system: role of the core planar cell polarity genes. *Nat Rev Neurosci*. 2013;14:525–35.
10. Tissir F, Qu Y, Montcouquiol M, Zhou L, Komatsu K, Shi D, et al. Lack of cadherins *Celsr2* and *Celsr3* impairs epiphyseal ciliogenesis, leading to fatal hydrocephalus. *Nat Neurosci*. 2010;13:700–7.
11. Qu Y, Glasco DM, Zhou L, Sawant A, Ravni A, Fritzsch B, et al. Atypical cadherins *Celsr1-3* differentially regulate migration of facial branchiomotor neurons in mice. *J Neurosci*. 2010;30:9392–401.
12. Qu Y, Huang Y, Feng J, Alvarez-Belado G, Grove EA, Yang Y, et al. Genetic evidence that *Celsr3* and *Celsr2*, together with *Fzd3*, regulate forebrain wiring in a *Vangl*-independent manner. *Proc Natl Acad Sci USA* 2014;111:E2996–3004.
13. Shima Y, Kengaku M, Hirano T, Takeichi M, Uemura T. Regulation of dendrite maintenance and growth by a mammalian 7-pass transmembrane cadherin. *Dev Cell*. 2004;7:205–16.
14. Shima Y, Kawaguchi SY, Kosaka K, Nakayama M, Hoshino M, Nabeshima Y, et al. Opposing roles in neurite growth control by two seven-pass transmembrane cadherins. *Nat Neurosci*. 2007;10:963–9.
15. Schafer ST, Han J, Pena M, von Bohlen Und Halbach O, Peters J, Gage FH. The Wnt adaptor protein ATP6AP2 regulates multiple stages of adult hippocampal neurogenesis. *J Neurosci*. 2015;35:4983–98.
16. Tissir F, De-Backer O, Goffinet AM, Lambert, de Rouvroit C. Developmental expression profiles of *Celsr* (*Flamingo*) genes in the mouse. *Mech Dev*. 2002;112:157–60.
17. Wen Q, Weng H, Liu T, Yu L, Zhao T, Qin J, et al. Inactivating *Celsr2* promotes motor axon fasciculation and regeneration in mouse and human. *Brain*. 2022;145:670–83.
18. Takata A, Ionita-Laza I, Gogos Joseph A, Xu B, Karayiorgou M. De Novo synonymous mutations in regulatory elements contribute to the genetic etiology of Autism and Schizophrenia. *Neuron*. 2016;89:940–7.

19. Gulsuner S, Walsh T, Watts AC, Lee MK, Thornton AM, Casadei S, et al. Spatial and temporal mapping of de novo mutations in schizophrenia to a fetal prefrontal cortical network. *Cell*. 2013;154:518–29.
20. Bacchelli E, Loi E, Cameli C, Moi L, Vega-Benedetti AF, Blois S, et al. Analysis of a Sardinian multiplex family with autism spectrum disorder points to post-synaptic density gene variants and identifies CAPG as a functionally relevant candidate gene. *J Clin Med*. 2019;8:212.
21. Al-Mubarak B, Abouelhoda M, Omar A, AlDhalan H, Aldosari M, Nester M, et al. Whole exome sequencing reveals inherited and de novo variants in autism spectrum disorder: a trio study from Saudi families. *Sci Rep*. 2017;7:5679.
22. Vilboux T, Malicdan MC, Roney JC, Cullinane AR, Stephen J, Yildirimli D, et al. CELSR2, encoding a planar cell polarity protein, is a putative gene in Joubert syndrome with cortical heterotopia, microphthalmia, and growth hormone deficiency. *Am J Med Genet A*. 2017;173:661–6.
23. Feng G, Mellor RH, Bernstein M, Keller-Peck C, Nguyen QT, Wallace M, et al. Imaging neuronal subsets in transgenic mice expressing multiple spectral variants of GFP. *Neuron*. 2000;28:41–51.
24. Madisen L, Zwingman TA, Sunkin SM, Oh SW, Zariwala HA, Gu H, et al. A robust and high-throughput Cre reporting and characterization system for the whole mouse brain. *Nat Neurosci*. 2010;13:133–40.
25. Lagace DC, Whitman MC, Noonan MA, Ables JL, DeCarolis NA, Arguello AA, et al. Dynamic contribution of nestin-expressing stem cells to adult neurogenesis. *J Neurosci*. 2007;27:12623–9.
26. Tripodi M, Evers JF, Mauss A, Bate M, Landgraf M. Structural homeostasis: compensatory adjustments of dendritic arbor geometry in response to variations of synaptic input. *PLoS Biol*. 2008;6:e260.
27. Tavosanis G. Dendritic structural plasticity. *Dev Neurobiol*. 2012;72:73–86.
28. Lüthi A, Schwyzer L, Mateos JM, Gähwiler BH, McKinney RA. NMDA receptor activation limits the number of synaptic connections during hippocampal development. *Nat Neurosci*. 2001;4:1102–7.
29. Liu XD, Ai PH, Zhu XN, Pan YB, Halford MM, Henkemeyer M, et al. Hippocampal Lnx1-NMDAR multiprotein complex mediates initial social memory. *Mol Psychiatry*. 2021;26:3956–69.
30. Zoicas I, Kornhuber J. The role of the N-Methyl-D-Aspartate receptors in social behavior in rodents. *Int J Mol Sci*. 2019;20:5599.
31. Duffney LJ, Zhong P, Wei J, Matas E, Cheng J, Qin L, et al. Autism-like deficits in Shank3-deficient mice are rescued by targeting actin regulators. *Cell Rep*. 2015;11:1400–13.
32. Guo D, Peng Y, Wang L, Sun X, Wang X, Liang C, et al. Autism-like social deficit generated by Dock4 deficiency is rescued by restoration of Rac1 activity and NMDA receptor function. *Mol Psychiatry*. 2021;26:1505–19.
33. Gao FB, Kohwi M, Brennan JE, Jan LY, Jan YN. Control of dendritic field formation in Drosophila: the roles of flamingo and competition between homologous neurons. *Neuron*. 2000;28:91–101.
34. Kremer MC, Christiansen F, Leiss F, Paehler M, Knapek S, Andlauer TF, et al. Structural long-term changes at mushroom body input synapses. *Curr Biol*. 2010;20:1938–44.
35. Cline H, Haas K. The regulation of dendritic arbor development and plasticity by glutamatergic synaptic input: a review of the synaptotrophic hypothesis. *J Physiol*. 2008;586:1509–17.
36. Lee LJ, Lo FS, Erzurumlu RS. NMDA receptor-dependent regulation of axonal and dendritic branching. *J Neurosci*. 2005;25:2304–11.
37. Singh AP, VijayRaghavan K, Rodrigues V. Dendritic refinement of an identified neuron in the Drosophila CNS is regulated by neuronal activity and Wnt signaling. *Development*. 2010;137:1351–60.
38. Zou DJ, Cline HT. Postsynaptic calcium/calmodulin-dependent protein kinase II is required to limit elaboration of presynaptic and postsynaptic neuronal arbors. *J Neurosci*. 1999;19:8909–18.
39. Rocha M, Sur M. Rapid acquisition of dendritic spines by visual thalamic neurons after blockade of N-methyl-D-aspartate receptors. *Proc Natl Acad Sci USA*. 1995;92:8026–30.
40. Goffinet AM, Tissir F. Seven pass Cadherins CELSR1-3. *Semin Cell Dev Biol*. 2017; 69:102–10.
41. Nagaoka T, Ohashi R, Inutsuka A, Sakai S, Fujisawa N, Yokoyama M, et al. The Wnt/planar cell polarity pathway component Vangl2 induces synapse formation through direct control of N-cadherin. *Cell Rep*. 2014;6:916–27.
42. Nagaoka T, Kishi M. The planar cell polarity protein Vangl2 is involved in post-synaptic compartmentalization. *Neurosci Lett*. 2016;612:251–5.
43. Okerlund ND, Stanley RE, Cheyette BN. The planar cell polarity transmembrane protein Vangl2 promotes dendrite, spine and glutamatergic synapse formation in the mammalian forebrain. *Mol Neuropsychiatry*. 2016;2:107–14.
44. Dos-Santos Carvalho S, Moreau MM, Hien YE, Garcia M, Aubailly N, Henderson DJ, et al. Vangl2 acts at the interface between actin and N-cadherin to modulate mammalian neuronal outgrowth. *Elife*. 2020;9:e51822.
45. Hida Y, Fukaya M, Hagiwara A, Deguchi-Tawarada M, Yoshioka T, Kitajima I, et al. Prickle2 is localized in the postsynaptic density and interacts with PSD-95 and NMDA receptors in the brain. *J Biochem*. 2011;149:693–700.
46. Sowers LP, Loo L, Wu Y, Campbell E, Ulrich JD, Wu S, et al. Disruption of the non-canonical Wnt gene PRICKLE2 leads to autism-like behaviors with evidence for hippocampal synaptic dysfunction. *Mol Psychiatry*. 2013;18:1077–89.
47. Thakar S, Wang L, Yu T, Ye M, Onishi K, Scott J, et al. Evidence for opposing roles of Celsr3 and Vangl2 in glutamatergic synapse formation. *Proc Natl Acad Sci USA*. 2017;114:E610–E8.
48. Feng B, Freitas AE, Gorodetski L, Wang J, Tian R, Lee YR, et al. Planar cell polarity signaling components are a direct target of β-amyloid-associated degeneration of glutamatergic synapses. *Sci Adv*. 2021;7:eaabh2307.

ACKNOWLEDGEMENTS

We thank Yuying Li for technical assistance with WB experiments.

AUTHOR CONTRIBUTIONS

BC, KZ, HC, and WN performed mice crossing, behavioral tests, and histological studies. LW and BJ performed the electrophysiological studies. XL performed primary neuron culture experiments. ZS performed molecular assays. BC, JW, and CL carried out *in vivo* imaging and stereotaxic injection and analyzed data. JD, DW, and CP assisted in the behavioral tests. LZ assisted in the design and analysis of calcium recording assay. YQ, BJ, TY, KS, and LBZ designed and supervised the project. The manuscript was prepared by YQ, TY, BJ, and BC with input from all authors.

FUNDING

This work was supported by National Science and Technology Innovation 2030 Major Project of China (2021ZD0203900). This study was also supported by National Natural Science Foundation of China (82071261, 31671067 and U1801287 to Y.Q.), Key-Area Research and Development Program of Guangdong Province (2018B030340001) to YQ, Guangdong Natural Science Funds for Distinguished Young Scholars (2016A030306001) to YQ, and Guangdong Province Special Support Program (2015TQ01R837) to YQ, National Natural Science Foundation of China (81870869, 41030830 to BJ), Guangdong Key Project in "Development of new tools for diagnosis and treatment of Autism" (2018B030335001) to BJ, Research and Development Plan of Key Areas of Guangzhou Science and Technology Bureau (2020070030001) to BJ, and Open Research Funds of State Key Laboratory of Ophthalmology (2020KFO8) to BJ.

COMPETING INTERESTS

The authors declare no competing interests.

ADDITIONAL INFORMATION

Supplementary information The online version contains supplementary material available at <https://doi.org/10.1038/s41380-022-01664-x>.

Correspondence and requests for materials should be addressed to Bin Jiang, Ti-Fei Yuan or Yibo Qu.

Reprints and permission information is available at <http://www.nature.com/reprints>

Publisher's note Springer Nature remains neutral with regard to jurisdictional claims in published maps and institutional affiliations.